Directional Radio Channel Measurements at Mobile Station in Different Radio Environments at 2.15 GHz

Kimmo Kalliola[1,3], Heikki Laitinen[2], Kati Sulonen[1], Lasse Vuokko[1], and Pertti Vainikainen[1]

[1]Helsinki University of Technology
Institute of Digital Communications, Radio Laboratory
P.O. Box 3000, FIN-02015 HUT, Finland
e-mail: kimmo.kalliola@hut.fi

[2]VTT Information Technology, Telecommunications
P.O. Box 1201, FIN-02044 VTT, Finland

[3]Nokia Research Center, Radio Communications
P.O. Box 407, FIN-00045 Nokia Group, Finland

Abstract

We have performed extensive radio channel measurements in different radio environments at 2.15 GHz frequency. A spherical array and a wideband radio channel sounder were utilized at the mobile station in order to characterize the spatial radio channel at the mobile. The measurement setup, presented in [1], enables the full 3D spatial and polarization characterization of the wideband mobile radio channel in real-time. Based on the comprehensive dataset of over 300.000 snapshots collected along over 9 km of measurement routes we present the cross-polarization power ratio and average elevation power distribution at the mobile station in different radio environments. We also present some interesting examples showing variation of the local azimuth and elevation power distributions when the mobile moves in the urban environment. The examples demonstrate the effectiveness of the measurements in characterizing the radio propagation in difficult radio environments.

1 Introduction

Realistic spatial radio channel models are required for the performance evaluation of wireless communication systems exploiting the spatial properties of the radio channel. Directional radio channel measurements in realistic environments are prerequisite for the verification of the models and for correct parameter selection. In this paper we concentrate on the directional radio channel at the mobile receiver by describing the average elevation power distribution and cross-polarization power ratio (XPR) in different radio environments. These characteristics determine the Mean Effective Gain (MEG) of a mobile handset antenna [2,3]. We also present some interesting examples of the local azimuth and elevation power distributions in urban micro- and macrocellular environments. These examples give insight to the dominant propagation mechanisms in the environment and demonstrate the effectiveness of this kind of measurements in characterizing the radio propagation in difficult radio environments.

2 Measurements

2.1 Measurement Setup

The measurements were performed using a spherical array of 32 dual-polarized antenna elements [1] and a complex wideband radio channel sounder [4]. A wideband signal was transmitted using a single antenna, and received separately with each of the 32 elements of the spherical array for both θ and ϕ polarizations, using a fast 64-channel RF switch. During the measurements the transmitting antenna was placed in fixed locations corresponding to typical base station (BS) antenna installations in different cellular radio network configurations. A sectored BS antenna with 3 dB beamwidth of 80° in azimuth and 28° in elevation was used in all cases except for the indoor picocell, where the transmit antenna was omnidirectional. Transmitted polarization was always linear vertical. The spherical array acting as the mobile station (MS) was connected to the receiver of the sounder and moved along the measurement routes using a trolley or a car. The center of the array was at height of 1.7 m

above ground level. Approximately five snapshots of the received signal were sampled and stored per each wavelength the mobile moved, except for the highway macrocell, where the number of snapshots per wavelength was between two and three.

2.2 Channel Sounder

We used the wideband radio channel sounder developed at Helsinki University of Technology (HUT), Institute of Digital Communications (IDC) [4]. In the transmitter, a cyclic pseudo-noise sequence (m-sequence) modulates the carrier at 2.154 GHz. The chip frequency of the m-sequence was 30 MHz in all measurements leading to a delay resolution of 33 ns. The sequence length was adjusted according to the maximum excess delay in each environment to minimize the amount of produced data. The two used delay windows were 4.2 μs (indoor and microcell) and 8.5 μs (macrocell). In the receiver, the demodulated signal is divided into I- and Q- branches and sampled with two 120 Msps A/D-converters. Sequential sampling at a period equal to multiple sequence lengths enables continuous measurement at a high instantaneous sampling rate. The signal samples from each branch of the switch are then stored for off-line processing to compute the temporal and spatial information.

2.3 Post-processing of Data

The delays, directions-of-arrival (DoAs), amplitudes, and phases of both vertically (VP) and horizontally (HP) polarized components of the incoming waves at each snapshot were found through sequential delay-domain and angular-domain processing. Delay-domain processing involves the correlation of the received signal of each antenna element with a replica of the transmitted m-sequence, which yields the complex impulse response, and finding the local maxima of the power delay profile (PDP). In the angular-domain processing at most four multipaths per delay tap were separated using beamforming, as described in [1], with a grid of 2° in both elevation and azimuth. The DoA assigned to each multipath was the location of the beam maximum. To reject spurious components, only such multipaths were accepted for which the excess delay did not change more than ±1 samples (±8.3 ns), and the DoA more than 15° between subsequent snapshots. In addition, components with lifetimes less than five snapshots were rejected. As a result, we obtained for each measurement snapshot the angle resolved impulse response, defined as:

$$\begin{bmatrix} h^{\theta}(\theta,\phi,\tau) \\ h^{\phi}(\theta,\phi,\tau) \end{bmatrix} = \sum_{l=1}^{L} \begin{bmatrix} \alpha_l^{\theta} \\ \alpha_l^{\phi} \end{bmatrix} \delta(\theta-\theta_l)\delta(\phi-\phi_l)\delta(\tau-\tau_l) \quad (1)$$

where h^{θ} and h^{ϕ} denote the VP and HP components of the impulse response, respectively. θ_l and ϕ_l are the elevation and azimuth angles of l^{th} multipath, and τ_l is the excess delay.

2.4 Description of Measurement Environments

We performed measurements in five different radio environments. The environments, the approximate total route lengths, and the numbers of collected snapshots are presented in Table 1. The characteristic features of each environment are briefly described below.

The indoor picocell measurements were carried out in the transit hall of Helsinki airport. The omnidirectional BS antenna was elevated at 4.6 m above the floor level, and located so that the visibility over the hall was good. The BS–MS distance varied within 10...150 m. The portion of line-of-sight (LOS) measurements was significant, of the order of 40 %.

The outdoor–indoor measurements were performed in two different office buildings, both having four floors, and office rooms next to the outer walls made of brick. In both sites the BS antenna was placed on the rooftop of the neighboring building (distance less than 50 m). The BS antenna was approximately 3 and 8 m above the mobile antenna for the two sites. The measurement routes include both corridors and office rooms, and the ceiling height is in the range of 2.5...3 m in both buildings.

Table 1. Amount of collected data.

Environment	*Route length*	*Snapshots*
Indoor picocell (Airport)	260 m	N = 9 800
Outdoor – Indoor (Office)	220 m	N = 8 300
Urban microcell (h_{BS} =3/8/13 m)	3×1200 m = 3600 m	3×51 000 N=153 000
Urban macrocell (h_{BS} = 21/27 m)	2560 m	N=100 600
Highway macrocell	~2500* m	N = 47 600
TOTAL	~9140 m	N=319 300

*~2.5 samples per wavelength

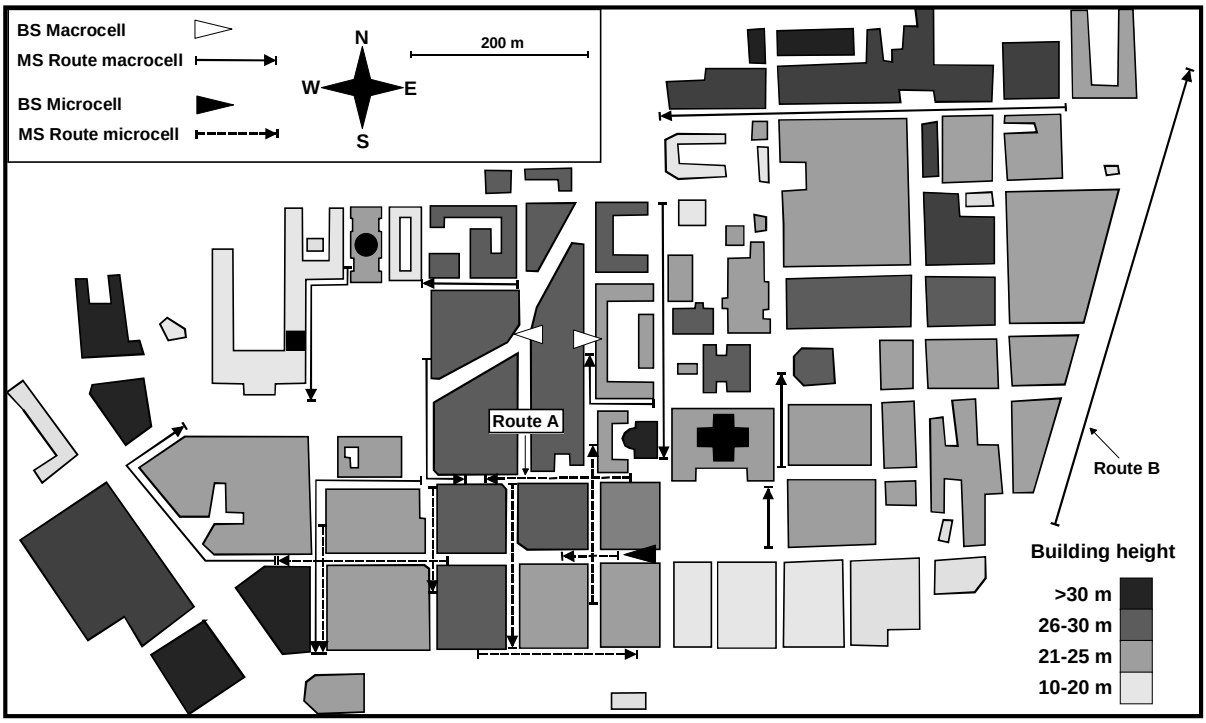

Fig. 1. Measurement routes in the center of Helsinki.

The urban micro- and macrocell measurements were performed in the center of Helsinki. The spherical array was located on a trolley, and the routes were driven along the sidewalks of the streets. Fig. 1 presents a map showing the BS positions and the measured mobile routes. The street grid in the measurement area is fairly regular and the average street width is approximately 15 m. The height of most buildings is in the range of 20...30 m .

In the microcell environment the same mobile routes were measured for the same base station location with three different antenna heights. The BS antenna was located on the sidewalk of a street, and mounted on a person lift elevated at 3, 8, and 13 m above the street level. The main beam of the antenna pointed west along the street. The measurement routes included the LOS main street, the two parallel streets on both sides, and four transversal streets in front of the antenna (see Fig. 1). The BS−MS distance varied within 10...350 m.

In the urban macrocell measurements the BS antenna was located on the rooftop of a parking house and pointed separately to two opposite directions in order to cover larger area (see Fig. 1). The antenna heights from ground were 27 and 21 m, the former being at, and the latter above the rooftop level of the opposite buildings. Photographs showing the views from both macrocell antenna installations can be found in [5]. The BS−MS distance varied within 50...750 m.

The highway macrocell measurements were carried out in an industrial area in Espoo, Finland. The BS antenna was located on top of a building next to a junction of a ring road with a lot of traffic. The BS antenna height was 17 m. During the measurements the spherical array was mounted inside a person car, as presented in Fig. 2. The measurement routes included the transversal ring road, and the crossing road. The BS−MS distance varied within 50...1200 m.

Fig. 2. Spherical array mounting in highway macrocell measurements.

3 Results

3.1 XPR

The XPR is defined as the power ratio of the VP and HP components of the incident field in the case of vertically polarized transmission. The measurement results indicate that the instantaneous XPR is lognormally distributed in all environments. Fig. 3 presents two examples of measured XPR distributions. The mean values of the two distributions are very close to each other, but the distribution is clearly wider in the outdoor-indoor measurements than in the urban microcell measurements. Table 2 presents the median (XPR_m), mean ($\overline{XPR}$), and the standard deviation (σ_{XPR}) of the cross polarization power ratio [in dB-scale] in different radio environments.

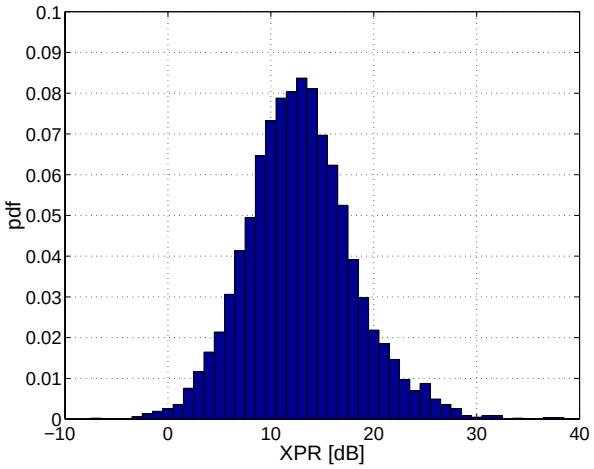

(a)

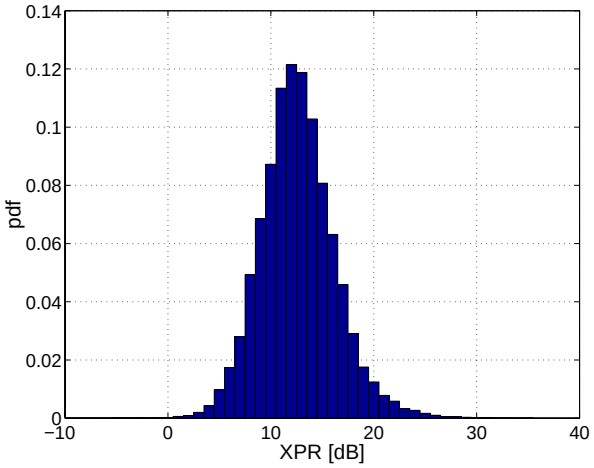

(b)

Fig. 3. Examples of measured XPR distributions. (a) indoor–outdoor, (b) urban microcell (h_{BS}= 8 m).

Table 2. XPR parameters.

Environment	XPR_m [dB]	$\overline{XPR}$ [dB]	σ_{XPR} [dB]
Indoor picocell	8.8	8.7	5.2
Outdoor – Indoor	12.7	12.9	5.2
Urban microcell:			
h_{BS} = 3 m	12.4	12.7	3.9
h_{BS} = 8 m	12.5	12.6	3.6
h_{BS} = 13 m	11.9	12.3	3.7
Urban macrocell	8.6	8.4	3.9
Highway macrocell	8.0	7.7	4.2

In the existing literature few measurements of the XPR at mobile station have been reported. Most of the research has concentrated on the BS end of the channel. In measurements by Lee [6] and Taga [1], the XPR in urban macrocells at MS has been between 4 dB and 9 dB at 900 MHz [1,6], which is slightly lower than what our results show at 2.15 GHz. The results are not completely comparable, however, since in our measurements both the antenna height and BS–MS distance were considerably smaller. The standard deviation of the XPR is clearly larger in indoors than in outdoor environments. Overall the reported XPR values are larger than what was expected based on previous work, especially in indoor environments.

3.2 Elevation Power Distribution

We computed the instantaneous elevation power distributions by summing the multipath powers for each 2-degree elevation angle bin, and normalizing the result by the total received power per snapshot. The distributions were computed separately for VP and HP signal components. The average elevation power distribution (EPD) of each environment was obtained by taking a mean over all snapshots in the environment. Fig. 4 presents the average elevation power distributions in different environments. The distributions have been multiplied by the mean relative incident VP and HP powers to emphasize the difference in the power levels. The parameters of the distributions: median (θ_m), mean ($\overline{\theta}$), and standard deviation (σ_θ) of the elevation angle are presented in Table 3.

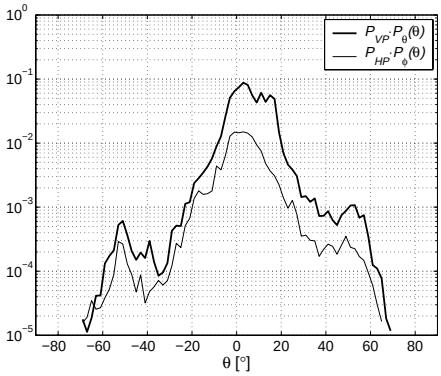

(a) indoor picocell

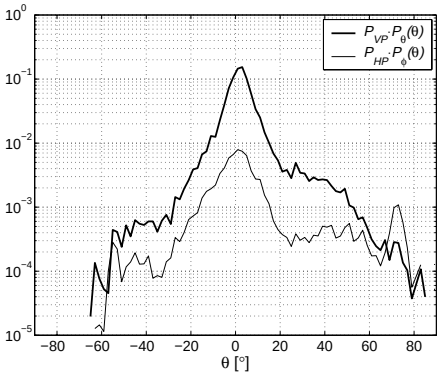

(b) outdoor – indoor

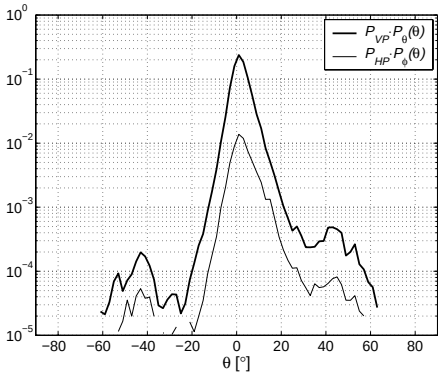

(c) urban microcell, h_{BS} = 3m

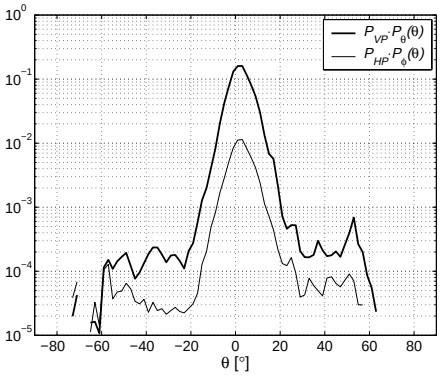

(d) urban microcell, h_{BS} = 8m

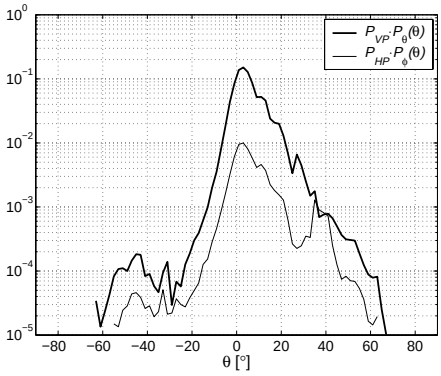

(e) urban microcell, h_{BS} = 13m

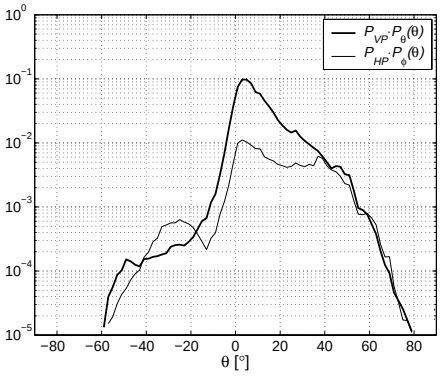

(f) urban macrocell

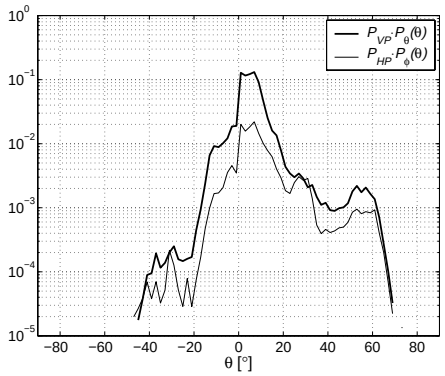

(g) highway macrocell

Table 3. EPD parameters (VP/HP).

Environment	θ_m	$\bar{\theta}$	σ_θ
Indoor picocell	4.1°/1.9°	6.0°/3.2°	10.3°/12.2°
Outdoor – Indoor	1.1°/0.7°	3.0°/6.3°	11.2°/23.0°
Urban microcell:			
h_{BS} = 3 m	0.6°/1.3°	2.1°/3.3°	5.4°/7.5°
h_{BS} = 8 m	1.2°/1.4°	2.4°/2.4°	6.4°/9.7°
h_{BS} = 13 m	3.2°/3.8°	5.7°/7.6°	8.0°/11.7°
Urban macrocell	6.8°/14.5°	11.1°/18.5°	12.2°/19.1°
Highway macro	4.3°/5.9°	6.4°/10.0°	9.8°/14.0°

Fig. 4. Average elevation power distribution at mobile station in different radio environments.

Fig. 4 demonstrates that the EPD clearly depends on the environment and BS antenna height. At least the following conclusions can be drawn:

1) In the indoor picocell measurements at the airport, significant portion of the mobile routes contain LOS, which can be seen in the vertically polarized EPD as peaks in the angle range of +10°...+20°. LOS routes make the main beam wider also in the highway macrocell measurements.

2) In urban outdoor measurements the distribution becomes asymmetrical when the BS antenna height increases, and more power is received at high elevation angles. The shape of the distribution for angles below horizon does not vary much. For large antenna heights also the XPR decreases when the elevation angle increases. In the urban macrocell case the XPR is approximately 0 dB for elevation angles above 40°.

3) In the outdoor–indoor measurements the received power outside the main lobe is significantly higher compared to the outdoor measurements, most likely due to reflections from the ceiling. An additional peak exists in the horizontally polarized EPD at a very high elevation angle (+72°). Similar effects can be seen also in the highway measurements, where the receiving antenna was inside a car.

3.3 Local Directional Power Distributions

We present two examples demonstrating the variation of the local directional power distributions when the mobile moves along a measurement route. Both examples are from the urban environment, one from the microcell, and the other from the macrocell measurements. The routes are marked in the map of Fig. 1 as 'Route A' and 'Route B'. The variation of the received power was removed from the results by normalizing the distributions to the total received power for each snapshot, in order to emphasize the directional behavior. The local distributions were then computed as an average over 10 snapshots (~2 wavelengths).

In the microcell example the BS antenna height was 3 m above ground. The route (Route A) was on the first parallel street to the north from the BS (see Fig. 1). The moving direction was from east to west. Figs. 5 and 6 present the local azimuth and elevation power distributions, respectively, along the route. The mobile moving direction is defined as 0° in the azimuth. Fig. 7 presents the local power delay profiles along the same route.

Fig. 5 shows that most of the energy is received from a few dominant secondary sources with relatively long lifetimes. The azimuth spreading due to scattering is of the order of 20 degrees around the source center directions. In addition to these dominant components, plenty of diffuse signal components exist, due to local scattering effects in the street canyon. The dominant secondary sources can be identified as the closest building block corners around the mobile. The first side street acts as a waveguide feeding the street along which the mobile is moving. This can be seen in Fig. 5, where the major DoA changes from right to left when bypassing the side street crossing (mobile location 33...47 m). At the same time the signal components on the right-hand side seem to disappear, which is due to the limited instantaneous dynamic range of the measurement system (approximately 30 dB). After the crossing the dominant secondary source is again at right. The diffraction from the side street corner at left also exists, but is much weaker. Similar behavior can be observed for the second side street (mobile location 128...150 m).

The effect of the side streets can be seen also in the elevation profile (Fig. 6). When bypassing the first crossing, no signal is received from elevation angles above 10°, presumably due to the slight downward slope of the side street. The mean elevation angle slightly decreases also when bypassing the second side street, conceivably due to more distant secondary sources. In other parts of the route most of the power is received from elevation angles below 20°, although the mobile traveled on a sidewalk only two meters from the building wall at left. This indicates that no signals propagate over building rooftops but the propagation takes place in street canyons. In the power delay profile, Fig. 7, two delay clusters can be identified, corresponding to propagation via the first and second side street. The mean excess delay and rms delay spread averaged over the route are 0.26 μs and 0.17 μs, respectively.

Our second example is from the urban macrocell, where the average distance between the BS and the mobile route (Route B) was approximately 600 m (see Fig. 1). The moving direction was to northeast. The route was on the seashore, and on the right-hand side the nearest buildings are on the opposite side of a bay, more than 500 m away from the mobile (not visible in Fig. 1). Figs. 8 and 9 present the local azimuth and elevation power distributions along the route. Fig. 10 presents the local power delay profiles along the same route.

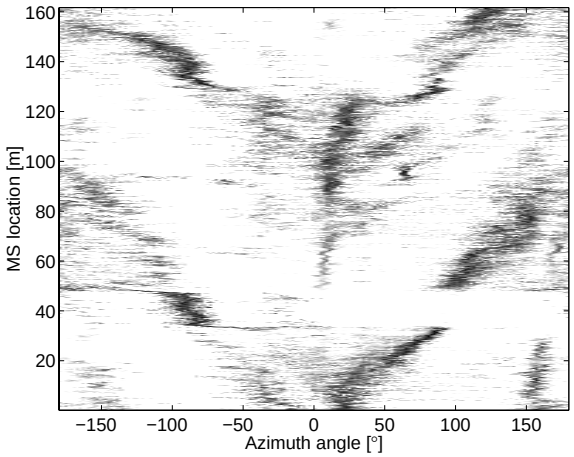

Fig. 5. Local azimuth power distribution along 'Route A' in Fig. 1. Mobile moving direction is 0°.

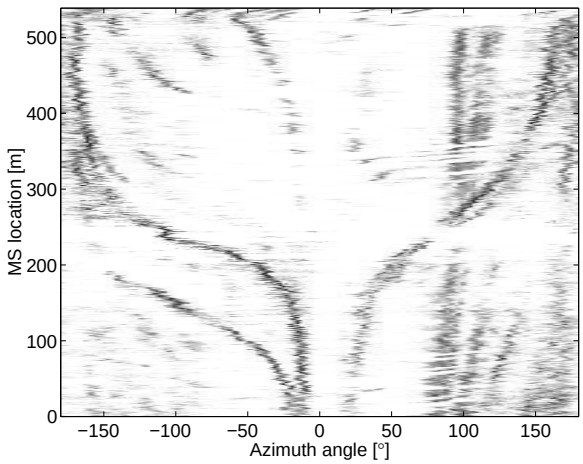

Fig. 8. Local azimuth power distribution along 'Route B' in Fig. 1. Mobile moving direction is 0°.

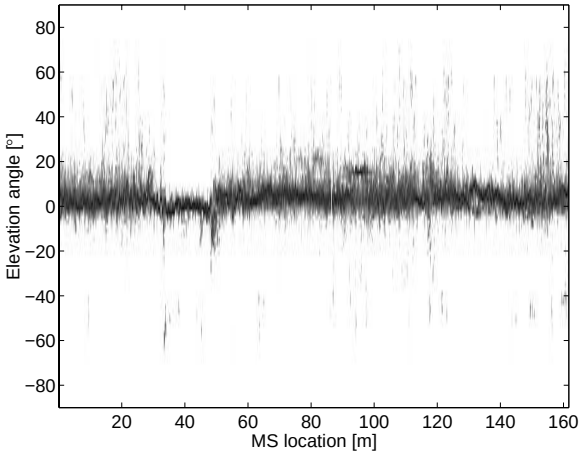

Fig. 6. Local elevation power distribution along 'Route A' in Fig. 1.

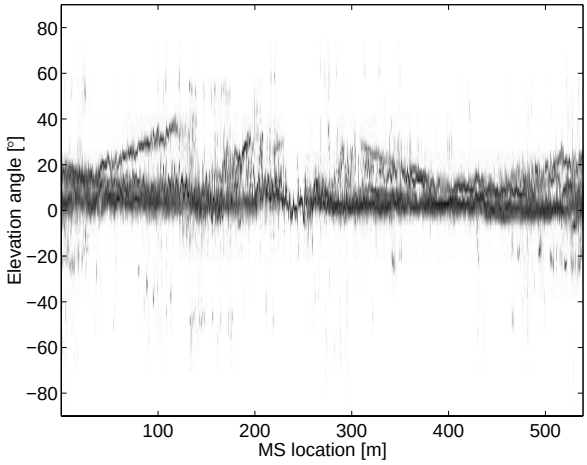

Fig. 9. Local elevation power distribution along 'Route B' in Fig. 1.

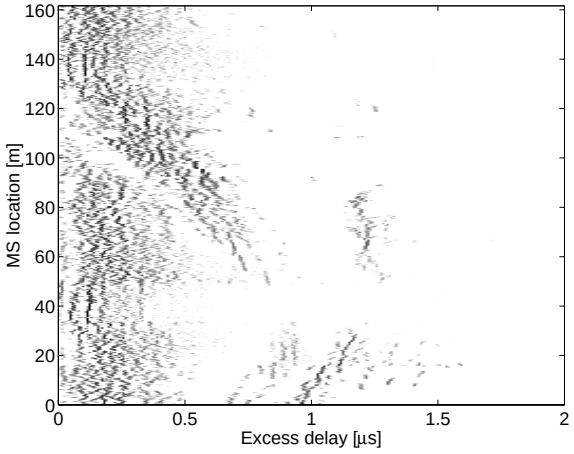

Fig. 7. Local power delay profile along 'Route A' in Fig. 1.

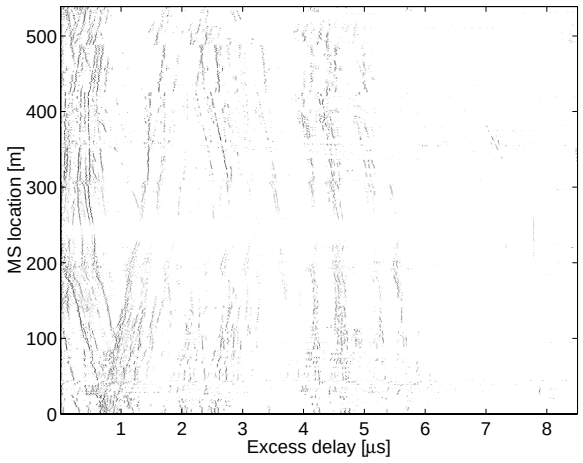

Fig. 10. Local power delay profile along 'Route B' in Fig. 1.

As in the microcell case, discrete dominant secondary sources with long lifetimes exist also in the macrocell case. The azimuth spreading is clearly smaller than in the microcell case, of the order of 10°. One of the dominant secondary sources corresponds to the crossing of the second side street approaching from left. There is a LOS from the BS to the upper corners of the buildings in the crossing. The strongest signal level on the route occurs when the mobile bypasses the crossing (mobile location 235...250 m), although a hill blocks the direct LOS path between BS and MS along the street. An image of the source can be observed at right, most probably originated from a boat attached to the pier opposite to the crossing. This component seems to disappear due to limited dynamic range when the mobile bypasses the crossing (see Figs. 8 and 10). Also traces of signals propagating via other street canyons at left (crossings at mobile locations 140...155 m and 430...445 m) can be found in Fig. 8. The other traces at right (azimuth angles +80...+120°) are reflections from a distant building cluster on the other side of the bay, to which there is a LOS from the BS. Due to the distant reflection points their azimuth directions change slowly along the route. These components are also clearly more diffuse due to scattering from the large building cluster. The elevation power distribution (Fig. 9) clearly shows the upper corners of buildings at left, as traces with varying elevation angle. The maximum elevation angles containing significant signal components are in the range of 30...40°, corresponding to the rooftop level of the buildings. In general more power is received from high elevation angles than in the microcell case where the BS antenna height was smaller. The signal components from the other side of the bay can be identified in the power delay profile, Fig. 10. These components form a separate cluster beginning approximately at the excess delay of 4 μs. As in the azimuth distribution, continuous signal traces can be seen also in the power delay profile. The mean excess delay and rms delay spread averaged over the route are 0.97 μs and 1.2 μs, respectively.

4 Conclusions

In this contribution we reported extensive directional radio channel measurements performed in different radio environments with a spherical array at the mobile station at 2.15 GHz frequency. We showed that the XPR at the mobile seems lognormally distributed with different mean and standard deviation in different environments. Highest XPR values were obtained in outdoor–indoor and urban microcell environments, where the mean XPR was between 12 and 13 dB. The variance of the XPR was largest in indoor measurements. We also demonstrated that the average elevation power distribution depends on the environment and BS antenna height. In addition, we presented two interesting examples showing variation of the local azimuth and elevation power distributions when the mobile moves in the urban environment. Both examples show that most of the energy is received from a few dominant secondary sources with relatively long lifetimes. In addition, diffuse scattering from local surroundings of the mobile exists. These illustrations clearly demonstrate the usefulness of the measurements in characterizing the radio propagation in difficult radio environments. In future work the existing dataset will provide a basis for comparison with existing propagation models.

5 Acknowledgements

This work was financially supported by the Graduate School in Electronics, Telecommunications and Automation (GETA), HPY Foundation, Nokia Foundation, Wihuri Foundation, and the Finnish Society of Electronics Engineers.

6 Literature

[1] K. Kalliola, H. Laitinen, L.I. Vaskelainen, and P. Vainikainen, “Real-time 3D Spatial-Temporal Dual-polarized Measurement of Wideband Radio Channel at Mobile Station”, *IEEE Transactions on Instrumentation and Measurement*, Vol. 49, No. 2, April 2000, pp. 439-448.

[2] T. Taga, “Analysis for mean effective gain of mobile antennas in land mobile radio environments,” *IEEE Transactions on Vehicular Technology*, Vol. 39, No. 5, May 1990, pp. 117-131.

[3] K. Sulonen, K. Kalliola, and P. Vainikainen, “Comparison of Evaluation Methods for Mobile Handset Antennas”, *Proceedings of Millennium Conference on Antennas & Propagation (AP2000)*, Davos, Switzerland, April 9-14, 2000.

[4] J. Kivinen, T. Korhonen, P. Aikio, R. Gruber, P. Vainikainen, S.-G. Häggman, “Wideband Radio Channel Measurement System at 2 GHz”, *IEEE Transactions on Instrumentation and Measurement*, Vol. 48, No. 1, February 1999, pp. 39-44.

[5] K. Kalliola, J. Laurila, M. Toeltsch, K. Hugl, P. Vainikainen, and E. Bonek, “3-D Directional Wideband Dual-polarized Measurement of Urban Mobile Radio Channel with Synthetic Aperture Technique”, *Proceedings of Millennium Conference on Antennas & Propagation (AP2000)*, Davos, Switzerland, April 9-14, 2000.

[6] W. C.–Y. Lee, "Polarization Diversity System for Mobile Radio", *IEEE Transactions on Communications*, vol. COM-20, No. 5, October 1972, pp. 912–923.

